



# Enhancement of the capacitance properties and the photoelectrochemical performances of P3HT film by incorporation of nickel oxide nanoparticles

Yasser Ghalmi<sup>1</sup> · Farid Habelhames<sup>1</sup> · Abdelfetteh Sayah<sup>1</sup> · Ahmed Bahloul<sup>1</sup> · Balkacem Nessark<sup>1</sup> · Hassina Derbal-Habak<sup>2</sup> · Yvan Bonnassieux<sup>3</sup> · Jean-Michel Nunzi<sup>4</sup>

Received: 21 July 2018 / Revised: 16 October 2018 / Accepted: 31 October 2018 / Published online: 15 November 2018  
© Springer-Verlag GmbH Germany, part of Springer Nature 2018

## Abstract

P3HT films were modified by incorporation of different amounts of nickel oxide (NiO). The nickel oxide powder was synthesized by chronoamperometry. The composites were further dissolved and deposited by the spin-coating method on indium-tin oxide (ITO) substrates. Effects of NiO content on the morphology structure and optical properties of P3HT films were investigated by means of XRD, SEM, AFM, and UV–Vis spectroscopy. Electrochemical and photoelectrochemical performances were evaluated by cyclic voltammetry (CV), electrochemical impedance spectroscopy (EIS), galvanostatic charge–discharge, and photocurrent measurements. Results show that NiO dispersed uniformly in P3HT thin films and modified the surface roughness and absorption of the deposited thin films. A remarkable improvement of photocurrent density and electrochemical capacitance is observed for an NiO content ranging between 1 and 10 wt%. The specific capacitance obtained for P3HT alone is about  $20.8 \text{ F g}^{-1}$ , this value increases to  $81.4 \text{ F g}^{-1}$  for the P3HT–NiO 10 wt% composite film at  $0.1\text{-A/g}$  current density.

**Keywords** NiO · P3HT · Composite film · Photocurrent · Supercapacitors

## Introduction

In recent years, the increasing demand for renewable energy resources received a major attention. In order to tackle the

problem, researchers also focused on organic photovoltaic (OPV) devices which seem to be one possible solution for niche applications like connected objects. Organic photovoltaic (OPV) devices are easy to manufacture, low cost, lightweight, and ecofriendly when compared to more classical energy supplies. Additionally, OPV devices proved to be amenable to large area roll-to-roll manufacturing [1–3], supplementing energy storage systems such as electrochemical batteries and capacitors (ECs) [4–8].

Hybrid (organic–inorganic) composite materials are increasingly important owing to their versatile properties, which arise from the synergism between the properties of their constituents. These composite materials can be obtained by several methods, a simple one being the incorporation of inorganic semiconductors into organic polymers, in which inorganic semiconductor particles can have larger absorption coefficients and conductivity than organic semiconductor materials [9, 10]. Organic–inorganic composite materials have attracted significant interest due to the remarkable change in photoelectrochemical properties when compared to the pure organic polymers [11–14].

✉ Yasser Ghalmi  
ghalmiyasser@gmail.com

✉ Farid Habelhames  
habelhamesfarid@yahoo.fr

✉ Abdelfetteh Sayah  
sadjed19@yahoo.fr

<sup>1</sup> Laboratoire d'Electrochimie et Matériaux (LEM), Département de Génie des Procédés, Faculté de Technologie, Université Ferhat Abbas, 19000 Sétif 1, Algeria

<sup>2</sup> Laboratoire des Technologies Innovantes (LTI), Université de Jules Verne, IUT de l'Oise Allée de la Faïencerie, 60100 Creil, France

<sup>3</sup> Laboratoire de Physique des Interfaces et des Couches Minces, Ecole Polytechnique, CNRS UMR 7647, 91128 Palaiseau, France

<sup>4</sup> Department of Physics, Engineering Physics and Astronomy, Department of Chemistry, Queen's University, Kingston ON K7L-3N6, Canada

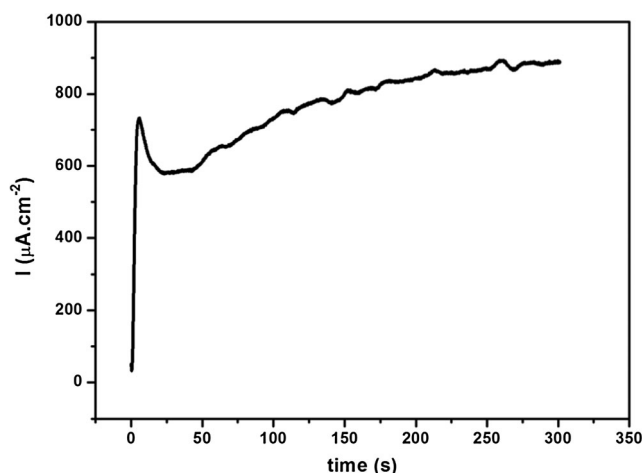


**Fig. 1** Chronoamperograms of NiO synthesis under 0.91 V vs. SCE cathodic potential

The most studied component of organic photovoltaic (OPV) devices is poly(3-hexylthiophene) (P3HT), which is still a subject of research in terms of electrochemical properties modification by addition or incorporation of other chemicals or particles [15–17]. So, several researchers have studied P3HT as an electron donor (p-type semiconductor) in OPVs for improve energy conversion efficiency [18–20] and recently, in supercapacitors due to its promising capacitive properties. An advantageous aspect of P3HT is the easiness to dissolve in a wide range of organic solvents, a fact that enables its deposition over large areas under different deposition techniques such as spray, spin, and dip coating [21, 22].

It was also reported that by modifying a P3HT polymer layer by using inorganic semiconductors materials like TiO<sub>2</sub>, ZnO, Fe<sub>3</sub>O<sub>4</sub>, CdS, CdSe, and WS<sub>2</sub>, the morphology, optical, and electrical properties of polymer layer could be improved [23–29].

Nickel oxide (NiO) is a p-type semiconductor with band gap energy in the 3.5–4.0 eV range [30]. A remarkable aspect of nickel oxide (NiO) that attracted researchers' attention [31] is its polyvalent use in many applications, i.e., transparent conducting films, anode buffer layer in OPVs [32], and electrochemical supercapacitors [33–38]. To produce NiO films, there are several technical available: sol–gel [30], chemical deposition [39], spray pyrolysis [40], thermal evaporation [41], sputtering [42], and electrodeposition [43] deserving special attention.

Among conducting polymers, poly(3-hexylthiophene) (P3HT), polythiophene (PTh), and polyaniline (PANI) with electron-donating properties are particularly used in supercapacitors applications. Electron flow from conducting polymers could be mitigated by the hybridization of the polymer with a high surface area material that has additional necessary properties to improve the overall capacitive performance of the final composite. The conducting polymers-electrode porous structure and material surface area are determinant for the optimum capacitance, which is due to the surface phenomena associated with supercapacitors [8, 37, 44].

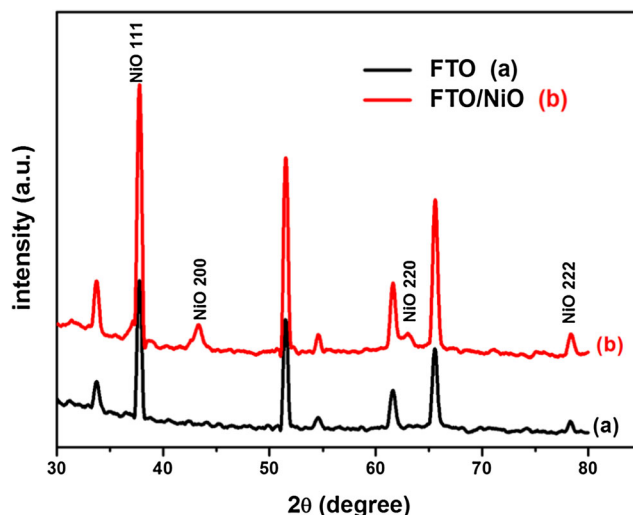


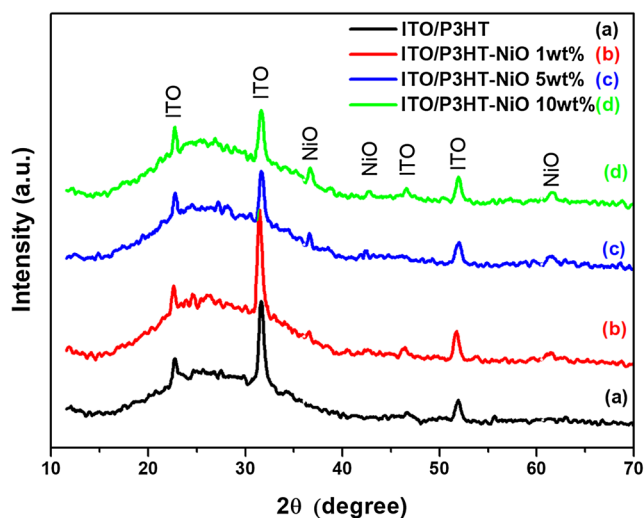
**Fig. 2** XRD spectra of FTO (a) and NiO (b)

In the present research, we prepared a P3HT-NiO composite material in which NiO was obtained through chronoamperometry. The NiO was then blended into P3HT in various proportions (1–10%) so that the P3HT-NiO composite could be spin coated on indium-tin oxide (ITO). The capacity and photoelectrochemical properties of the different composite films were respectively studied by galvanostatic charge/discharge and photocurrent measurement.

## Experimental

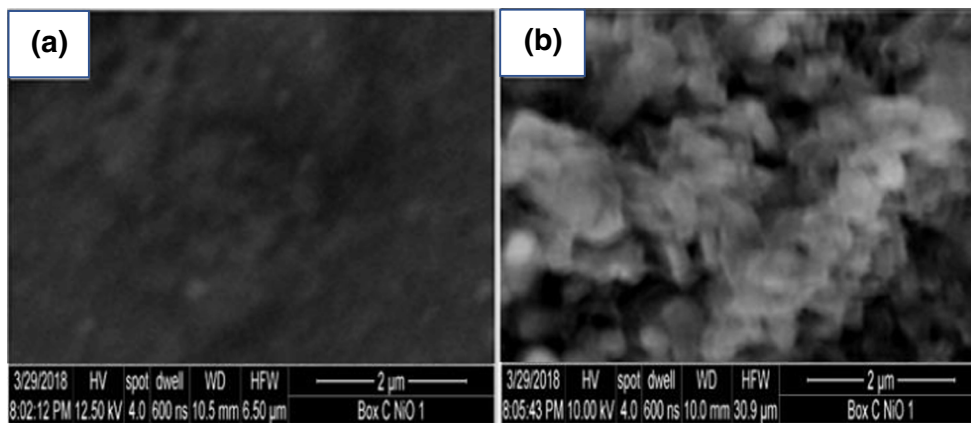
### Synthesis of the NiO powder

Figure 1 represents the electrochemically prepared NiO powder by applying a constant 0.91 V vs. SCE cathode potential on a fluorine-doped tin oxide (FTO)-coated glass used as



**Fig. 3** XRD spectra of ITO/P3HT (a), ITO/P3HT-NiO 1 wt% (b), ITO/P3HT-NiO 5 wt% (c), and ITO/P3HT-NiO 10 wt% (d)

**Fig. 4** SEM images of ITO/P3HT (a) and ITO/P3HT-NiO (b)



working electrode. A graphite rod and SCE counter electrode was used as reference electrode. The electrolyte was a solution of 0.1 M NiSO<sub>4</sub>·6H<sub>2</sub>O, 0.1 M Na<sub>2</sub>SO<sub>4</sub>, and 0.1 M CH<sub>3</sub>COONa in a water deionizer. The NiO deposit was cleaned with deionized water and scraped with a blade. The resulting powder was annealed for 1 h at 500 °C.

were ultrasound cleaned 15 min successively in deionized water, ethanol, and acetone.

P3HT containing different amounts of NiO (0–10 wt%) was dissolved in chlorobenzene (C<sub>6</sub>H<sub>5</sub>Cl) by stirring during 24 h and spin coated at 500 rpm for 30 s on ITO. Spin-coated films were annealed at 80 °C in air during 10 min.

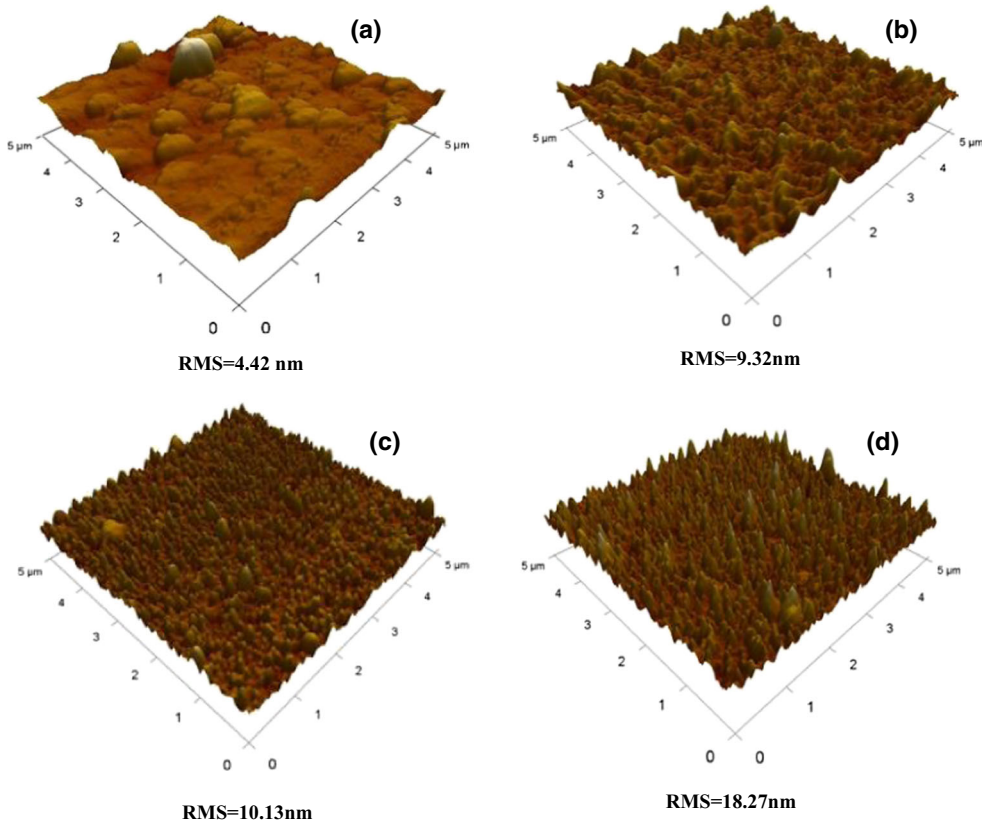
**P3HT-NiO thin films preparation**

ITO-coated glass substrates were obtained from SOLEMS. ITO thickness was 100 nm with about 25 Ω/sq resistivity and 93% average transmittance in the visible. ITO substrates

**Characterizations**

Electrochemical tests were carried out at normal environment temperature in one compartment cell by the use of PGZ-301 Voltalab connected to computer with voltmaster 4 operating

**Fig. 5** AFM images of ITO/P3HT (a), ITO/P3HT-NiO 1 wt% (b), ITO/P3HT-NiO 5 wt% (c), and ITO/P3HT-NiO 10 wt% (d)



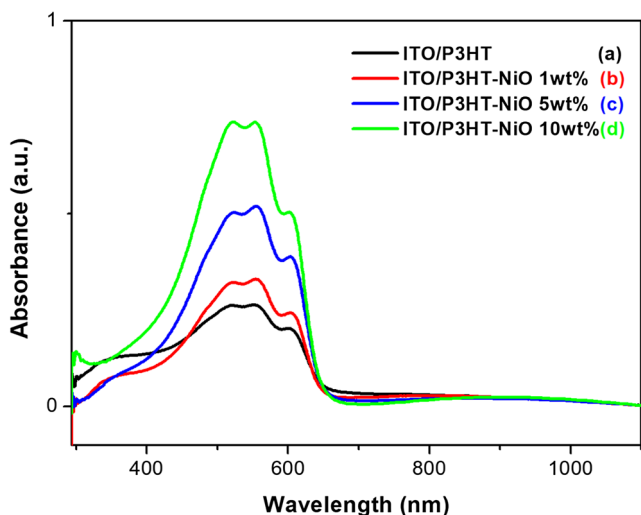


**Fig. 6** UV-visible spectra of ITO/P3HT (a), ITO/P3HT-NiO 1 wt% (b), ITO/P3HT-NiO 5 wt% (c), and ITO/P3HT-NiO 10 wt% (d)

software. The latter enables selection of the electrochemical technique under the aimed parameters. Electrochemical measurements were operated in a three-electrode cell with indium-tin oxide (ITO) as working electrode, saturated calomel

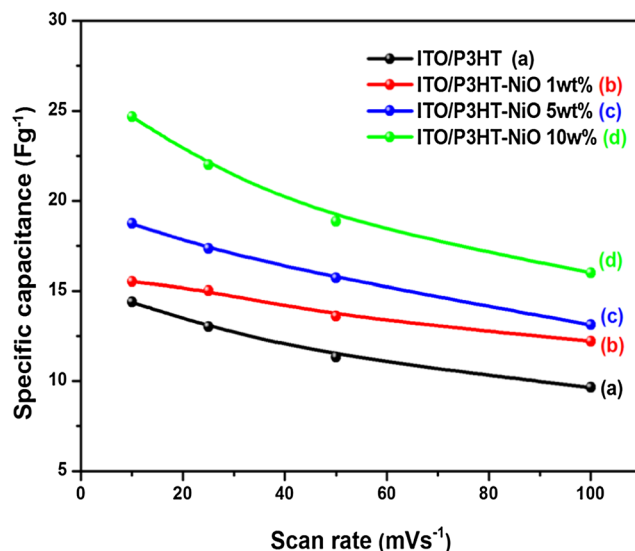


**Fig. 8** Specific capacitance of ITO/P3HT (a), ITO/P3HT-NiO 1 wt% (b), ITO/P3HT-NiO 5 wt% (c), and ITO/P3HT-NiO 10 wt% (d) obtained under different scan rates

electrode (SCE) as reference electrode, and a graphite rod as auxiliary electrode.

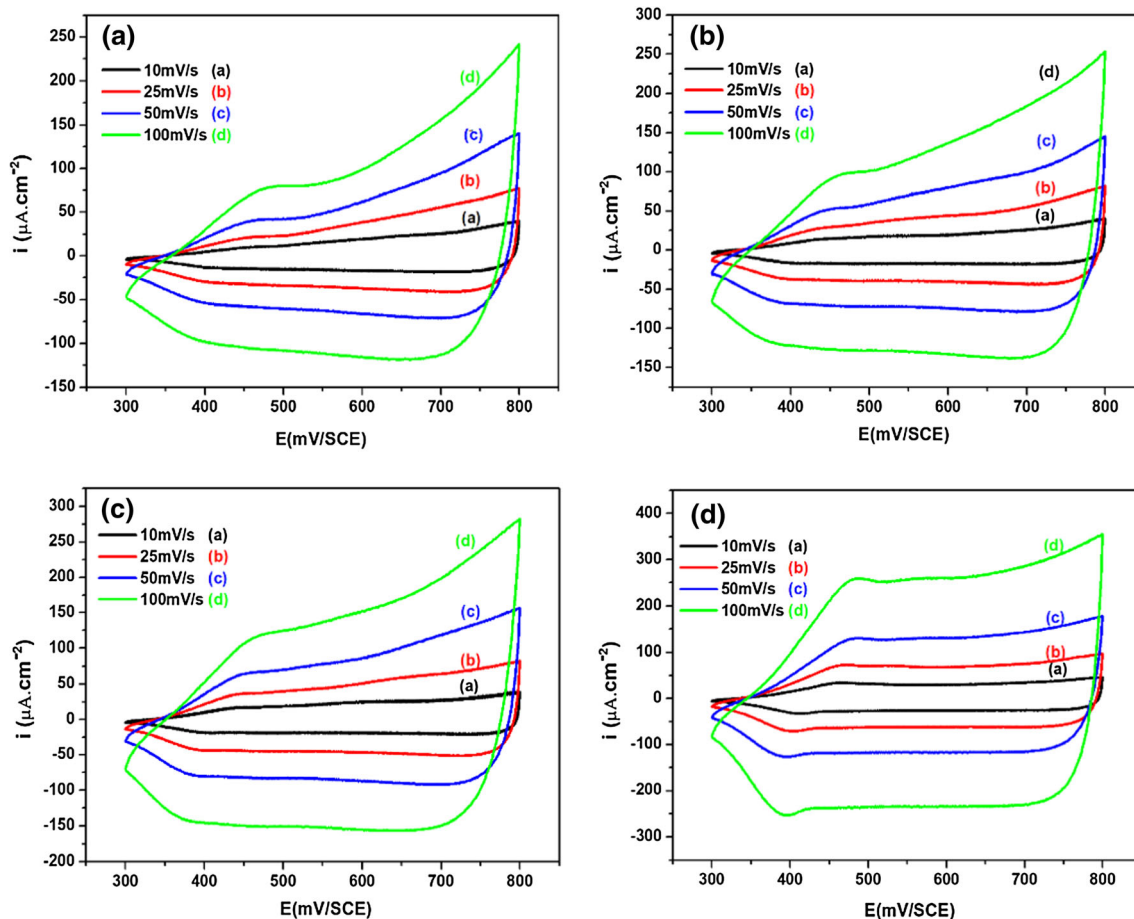


**Fig. 7** Cyclic voltammograms of ITO/P3HT (a), ITO/P3HT-NiO 1 wt% (b), ITO/P3HT-NiO 5 wt% (c), and ITO/P3HT-NiO 10 wt% (d), at different scan rates in 0.1 M  $\text{LiClO}_4/\text{CH}_3\text{CN}$  electrolyte

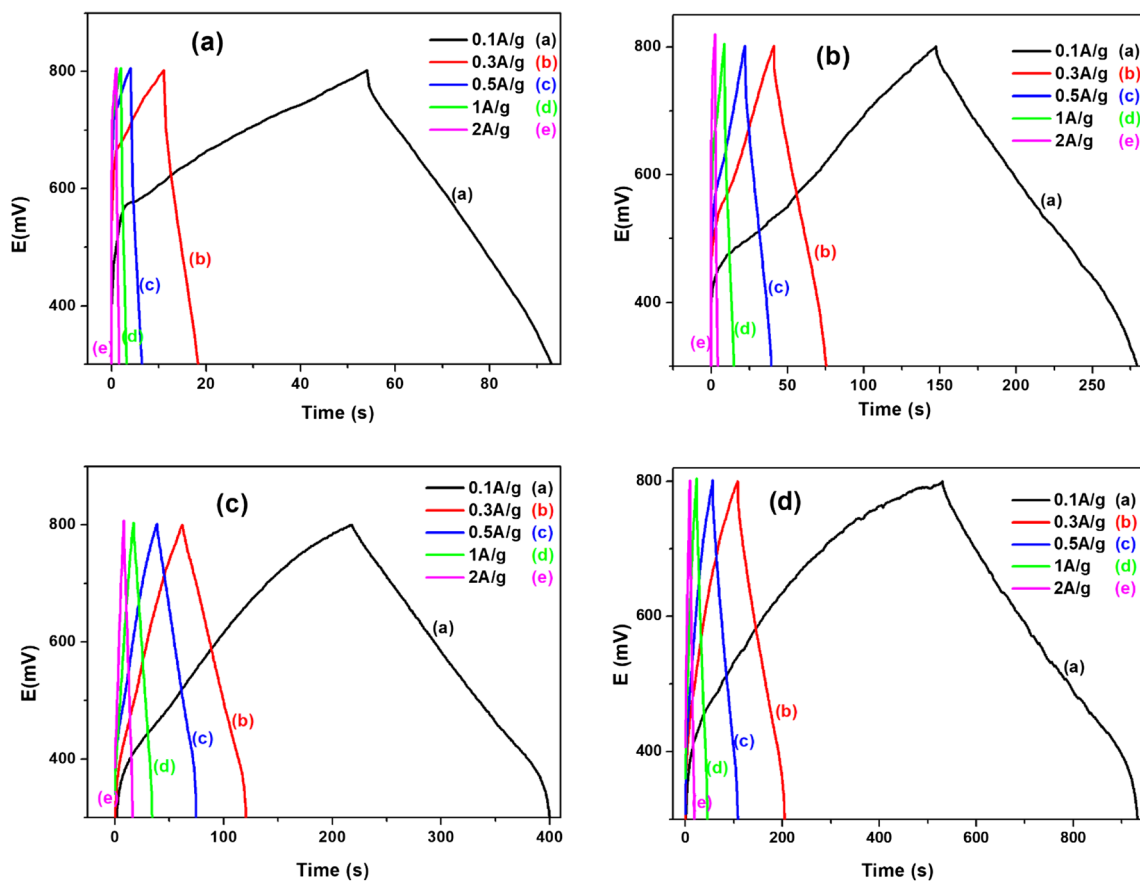


**Fig. 9** Galvanostatic charge–discharge curves of ITO/P3HT (a), ITO/P3HT-NiO 1 wt% (b), ITO/P3HT-NiO 5 wt% (c), and ITO/P3HT-NiO 10 wt% (d), at different current density, in 0.1 M LiClO<sub>4</sub>/CH<sub>3</sub>CN electrolyte, carried out from 0.3 to 0.8 V vs. SCE

The ITO/P3HT and ITO/P3HT-NiO (1, 5, and 10 wt%) thin films were examined under different techniques. XRD analysis was carried with a Rigaku powder X-ray diffractometer

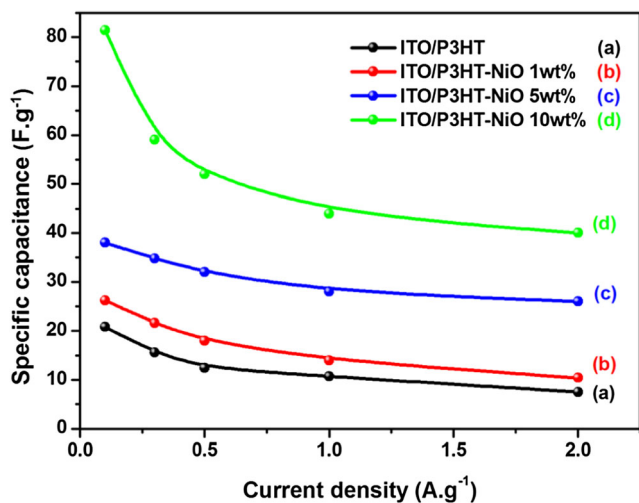


**Fig. 10** Specific capacitance of ITO/P3HT (a), ITO/P3HT-NiO 1 wt% (b), ITO/P3HT-NiO 5 wt% (c), and ITO/P3HT-NiO 10 wt% (d), at different current density

(model RINT 2100) with a CuK $\alpha$  source ( $\lambda = 1.54 \text{ \AA}$ ). UV–visible was then taken with a Shimadzu UV-1800 UV–VIS spectrophotometer. Atomic force microscopy (AFM) images were taken in the contact mode with a MFP 3D AFM from Asylum research. The images were used to quantify thin film roughness. Scanning electron microscopy (SEM) micrographs were obtained from a Neo Scope, JEOL, JCM-5000.

Photoelectrochemical tests were carried out in (LiClO<sub>4</sub> 0.1 M + CH<sub>3</sub>CN) electrolyte; the photocurrent was obtained after switching the lights on and off, with an applied potential of  $-1.2$  to  $+1$  V vs. SCE. The working electrode was irradiated with a 500-W white light lamp, in which intensity was measured using a Luxmeter testo-540 as  $100 \text{ Wm}^{-2}$ .

### Results and discussion

XRD in Fig. 2 shows peaks at  $2\theta = 37^\circ, 43^\circ,$  and  $62^\circ$ . The peak values are likely to be those characterizing the cubic NiO, in harmony with standard specific values, i.e., (JCPDS01-073-1519) [33, 43]. NiO grain size is figured out through XRD according to Debye–Scherrer’s law:

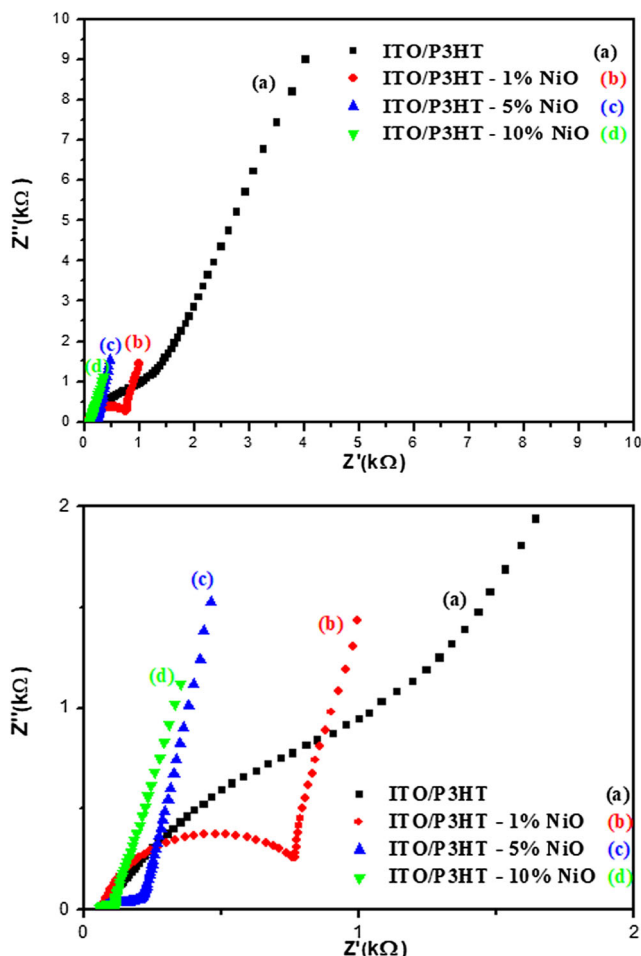


**Fig. 11** Nyquist plots of ITO/P3HT, ITO/P3HT-NiO 1 wt%, ITO/P3HT-NiO 5 wt%, and ITO/P3HT-NiO 10 wt%, in 0.1 M LiClO<sub>4</sub>/CH<sub>3</sub>CN electrolyte

$$D = 0.9\lambda/w \cos \theta \quad (1)$$

where  $D$  is grain size,  $\lambda$  is XRD wavelength,  $w$  is the full width half maximum, and  $\theta$  is the peak position. NiO grain size is estimated around 25 nm.

Figure 3 shows the XRD spectra of P3HT and P3HT-NiO (1–10%) composite films, where the peaks are shown at  $2\theta = 37^\circ$ ,  $43^\circ$ , and  $62^\circ$  as compared film without NiO. This confirms the incorporation of NiO nanoparticles in the P3HT films.

SEM images of composite films on ITO are shown in Fig. 4. The P3HT film in Fig. 4a presents smaller crystalline domains, with a nodular-like structure [45]. The

P3HT-NiO composite film consists in larger crystalline domains as compared to P3HT. Some material surrounding NiO clearly manifests, which is attributed to attach P3HT polymeric chains [46].

Figure 5 shows the AFM surface morphology of the P3HT and P3HT/NiO thin films. Surface roughness of the 0, 1, 5, and 10 wt% P3HT blends are respectively 4.42 nm, 9.32 nm, 10.13 nm, and 18.27 nm. Surface roughness increases under NiO addition up to 10 wt% in P3HT. The composite film exhibits a relatively sharp granular morphology with uniform grain size, suggesting the presence of a nanosized grain structure in the composite films [47–50]. It is recognized that surface morphology and device interfaces are of paramount importance for high-performance P3HT.

The optical spectra of NiO in P3HT are shown in Fig. 6. P3HT absorption is enhanced by 1–10 wt % NiO incorporation. The absorbance spectrum of pure P3HT film shows peaks at 610, 550, and 525 nm, which are in accordance with literature [51–53]. The absorption peak of the ITO/P3HT-NiO 10 wt% sample at 300 nm can be attributed to the cubic nickel oxide (NiO) [54–56]. This peak does not appear in the other spectra (1 and 5 wt%) owing to the low NiO concentration. NiO insertion clearly raises the overall absorbance of the film. This can be attributed to scattering by the NiO nanoparticles in which index of refraction is 2.1. This suggests an interaction between the NiO nanoparticles and P3HT.

Figure 7 shows the cyclic voltammograms of ITO/P3HT and ITO/P3HT-NiO (1, 5, and 10 wt%) composite films in the potential range of 0.3 to 0.8 V vs. SCE at various scan rates (10, 25, 50, 100 mV s<sup>-1</sup>). We notice that the CV curves of the electrode materials are nearly rectangular shaped [37]. Compared with the ITO/P3HT film, all ITO/P3HT-NiO composite films show an increase in the cyclic voltammetry charge–discharge areas, due to the increased NiO mass embedded into the polymer matrix.

The large cyclic voltammetry currents obtained for the ITO/P3HT-NiO 10 wt% composite film meaningfully shows a higher specific capacitance than ITO/P3HT, which is attributed to the rough surface of the ITO/P3HT-NiO composite films as compared to the ITO/P3HT film. The ITO/P3HT-NiO composite films show high electrical conductivity parameter, which is a prerequisite for supercapacitors. NiO present inside the polymer enables a high contact interface between P3HT and the electrolyte. The specific capacitance is evaluated using the following Eq. (2):

**Table 1** Impedance electrical parameters for ITO/P3HT, ITO/P3HT-NiO 1 wt%, ITO/P3HT-NiO 5 wt%, and ITO/P3HT-NiO 10 wt%

Element	ITO/P3HT	ITO/P3HT-NiO 1 wt%	ITO/P3HT-NiO 5 wt%	ITO/P3HT-NiO 10 wt%
$R_1$ ( $\Omega$ cm <sup>2</sup> )	65.16	50.24	61.08	63.77
$R_2$ ( $\Omega$ cm <sup>2</sup> )	4906	784	128	70.85
$Q_2$ ( $\mu$ F cm <sup>2</sup> )	68.98	$38 \times 10^{-5}$	$19.1 \times 10^{-1}$	$35.6 \times 10^{-1}$

**Fig. 12** Photocurrent response of ITO/P3HT (a), ITO/P3HT-NiO 1 wt% (b), ITO/P3HT-NiO 5 wt% (c), and ITO/P3HT-NiO 10 wt% (d), at -0.2 (A), -0.4 (B), -0.6 (C), -0.8 (D), -1 (E), and -1.2 V (F) vs. SCE in 0.1 M LiClO<sub>4</sub>/CH<sub>3</sub>CN electrolyte, observed upon switching the white lights on and off, at 100-mW cm<sup>-2</sup> light intensity

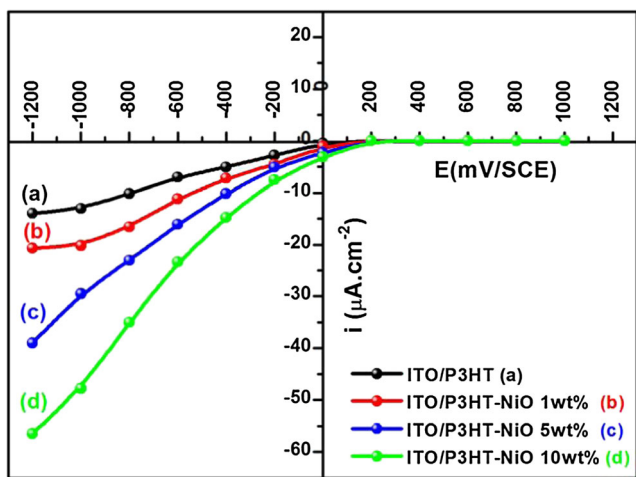
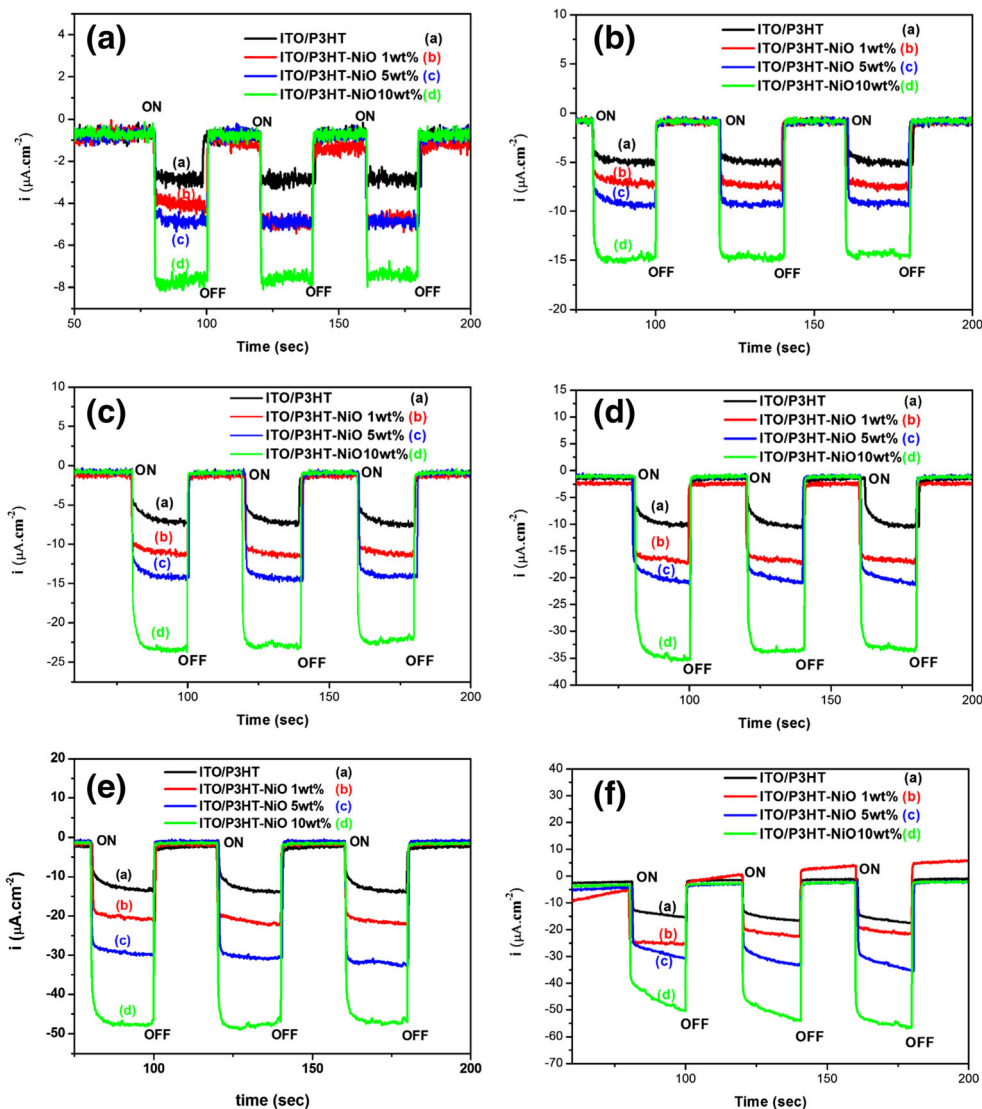


**Fig. 13** Photocurrent potential curve of ITO/P3HT (a), ITO/P3HT-NiO 1 wt% (b), ITO/P3HT-NiO 5 wt% (c), and ITO/P3HT-NiO 10 wt% (d), in the potential range -1.2 to 1 V vs. SCE in 0.1 M LiClO<sub>4</sub>/CH<sub>3</sub>CN electrolyte

$$SC = \frac{\int_{E_1}^{E_2} i(E)dE}{2(E_2-E_1)mv} \tag{2}$$

where SC is the specific capacitance,  $E_2-E_1$  is the potential window of cyclic voltammetry,  $\int_{E_1}^{E_2} i(E)dE$  is the voltammetric charge obtained by integration of the CV-curve,  $m$  is the deposited material weight on the working electrode, measured with 0.01-mg accuracy, and  $v$  is the scan rate.

The specific capacitance of ITO/P3HT and ITO/P3HT-NiO (1, 5, and 10 wt%) composite films obtained at different scan rates is given in Fig. 8. The ITO/P3HT film has a specific capacity of 14 F g<sup>-1</sup> at 10 mV/s. Upon NiO nanoparticle insertion, a significant increase in the specific capacitance happens with 16 F g<sup>-1</sup>, 19 F g<sup>-1</sup>, and 25 F g<sup>-1</sup>, respectively. The specific capacitance increase may be a direct consequence of the morphology changes upon NiO nanoparticle insertion.

Figure 9 shows the galvanostatic charge–discharge (GCD) curves of ITO/P3HT and the ITO/P3HT-NiO (1, 5, and 10 wt%) films at various current densities under voltages between 0.3 and 0.8 V vs. SCE. A typical charge–discharge curve is almost equilateral triangle shaped, which suggests a linear response to time potential in the charge–discharge process that witnesses good reversibility in the operation, indicating an excellent capacitive behavior. The electrode materials undergo two distinctive stages of voltage drop with quick discharge in the primary potential zone and some delay in the second potential zone. This has proven to be significant in terms of electrochemical performance.

Figure 10 represents the GCD plots of the electrode materials, set at current densities of 0.1, 0.2, 0.5, 1, and 2 A/g. It is found that the increase in the current density corresponds to the decrease in the discharge times of the electrode materials.

The ITO/P3HT-NiO 10 wt% composite films reaches the largest discharge time among the materials tested, witnessing its better specific capacitance. The specific capacitance (SC) of the studied electrode materials was calculated from the charge–discharge profile using Eq. (3):

$$SC = \frac{it}{m\Delta V} \quad (3)$$

where  $i/m$  is the current density used,  $\Delta V$  is the potential window, and  $t$  is the discharge time in seconds. The ITO/P3HT-NiO 10 wt% composite film reaches about 81.4 F/g specific capacitance at a 0.1-A/g current density. The ITO/P3HT, ITO/P3HT-NiO 1 wt%, and ITO/P3HT-NiO 5 wt% reach 20.8, 26.2, and 38 F/g capacitance values under the same applied current density of 0.1 A/g, as shown in Fig. 10. Increasing the current density causes a general decrease in a specific capacitance, which is understood as electrolyte ion depletion in the vicinity of the electrodes at higher current densities. Specific capacitance at different current densities was calculated from Eq. (2).

The impedance spectra of ITO/P3HT and ITO/P3HT-NiO composite films computed at open circuit potential (0.1 V vs. SCE) are displayed as Nyquist diagrams in Fig. 11. The films were studied in (LiClO<sub>4</sub> 0.1 M + CH<sub>3</sub>CN) solutions. The spectra were plotted in the 100 KHz to 50 MHz frequency band under 10-mV alternative voltage.

In the spectra, the semicircle diameter decreases with increasing NiO content in the P3HT matrix. This shows that electric conductivity decreases in the NiO composite films, from 4906  $\Omega$  cm<sup>2</sup> for ITO/P3HT to 784  $\Omega$  cm<sup>2</sup> for ITO/P3HT-NiO 1 wt%, 128  $\Omega$  cm<sup>2</sup> for ITO/P3HT-NiO 5 wt%, and 70.85  $\Omega$  cm<sup>2</sup> for ITO/P3HT-NiO 10 wt%. These values are reported in Table 1. Insertion of NiO in P3HT significantly increases the conductivity of the polymer.

Figure 12 shows the photocurrent amplitudes versus applied cathodic potential of the ITO/P3HT and ITO/P3HT-

NiO composite films under illumination. Tests were carried out in (LiClO<sub>4</sub> 0.1 M + CH<sub>3</sub>CN) electrolyte solution under an applied potential between 1.2 and 1 V vs. SCE for 100-mW/cm<sup>2</sup> light intensity. For all samples, both photocurrent and the depletion region increase with the applied cathodic potential. This is fully expected for a p-type semiconductor [12, 13, 20, 57, 58]. The photocurrent amplitude mostly increases with the NiO content of the composite film.

Figure 13 shows the photocurrent density as a function of the applied potential between –1.2 to 1 V vs. SCE for ITO/P3HT and ITO/P3HT-NiO electrodes with different NiO contents. The photocurrent is negative in all the potential range and it decreases with NiO content.

## Conclusion

Composite films of P3HT-NiO obtained by blending P3HT with various NiO amounts were deposited by spin coating on ITO substrates. It is shown that addition of NiO nanoparticles modified the morphology, spectroscopic and electrochemical properties of the P3HT film.

Moreover, the obtained specific capacity for the composite films (P3HT-NiO) was larger than that of the pure polymer, which is due to improved electronic conductivity. The specific capacitance for the P3HT material alone is about 20.8 F g<sup>-1</sup>, which is increased to 81.4 F g<sup>-1</sup> for the P3HT-NiO 10 wt% composite film at 0.1 A/g.

Our results also show that NiO nanoparticles improved the optical and photoelectrochemical response of the P3HT composite films. The photocurrent increases more than three times with 10% NiO nanoparticles in P3HT, thereby suggesting the use of this composite, an electron donor in OPVs.

## References

1. Strohm S, Machui F, Langner S, Kubis P, Gasparini N, Salvador M, McCulloch I, Egelhaaf HJ, Brabec CJ (2014) P3HT: non-fullerene acceptor based large area, semi-transparent PV modules with power conversion efficiencies of 5%, processed by industrially scalable methods. *Energy Environ Sci* 7:2792–2802. <https://doi.org/10.1039/C4EE01222D>.
2. Park S, Kim H, Kang Y, Kim D, Kang J (2010) Organic solar cells employing magnetron sputtered p-type nickel oxide thinfilm as the anode buffer layer. *Sol Energy Mater Sol Cells* 94:2332–2336. <https://doi.org/10.1016/j.solmat.2010.08.004>
3. Krebs F, Alstrup J, Spanggaard H, Larsen K, Kold E (2004) Production of large-area polymer solar cells by industrial silk screen printing, lifetime considerations and lamination with polyethyleneterephthalate. *Sol Energy Mater Sol Cells* 83:293–300. <https://doi.org/10.1016/j.solmat.2004.02.031>
4. Ruzmetov D, Oleshko V, Haney P, Lezec H, Karki K, Baloch K, Agrawal A, Davydov A, Krylyuk S, Liu Y, Huang J, Tanase M, Cumings J, Talin A (2012) Electrolyte stability determines scaling



- limits for solid-state 3DLi ion batteries. *Nano Lett* 12:505–511. <https://doi.org/10.1021/nl204047z>
5. Hall P, Mirzaeian M, Fletcher S, Sillars F, Rennie A, Shitta-Bey G, Wilson G, Cruden A CR (2010) Energy storage in electrochemical capacitors: designing functional materials to improve performance. *Energy Environ Sci* 3:1238–1251. <https://doi.org/10.1039/c0ee00004c>
  6. Simon P, Gogotsi Y (2008) Materials for electrochemical capacitors. *Nat Mater* 7(845–854):845–854. <https://doi.org/10.1038/nmat2297>
  7. Notten PHL, Roozeboom F, Niessen RAH, Baggetto L (2007) 3-D integrated all-solid-state rechargeable batteries. *Adv Mater* 19:4564–4567. <https://doi.org/10.1002/adma.200702398>
  8. Sayah A, Habelhames F, Bahloul A, Nessark B, Bonnassieux Y, Tendelier D, ElJouad M (2018) Electrochemical synthesis of polyaniline-exfoliated graphene composite films and their capacitance properties. *J Electroanal Chem* 818:26–34. <https://doi.org/10.1016/j.jelechem.2018.04.016>
  9. Arici E, Meissner D, Schäffler F, Sariciftci NS (2003) Core/shell nanomaterials in photovoltaics. *Int J Photoenergy* 5:199–208
  10. Fumagalli F, Bellani S, Schreier M, Leonardi S, Rojas HC, Ghadirzadeh A, Tullii G, Savoini A, Marra G, Meda L, Grätzel M, Lanzani G, Mayer MT, Antognazza MR, Fozzo FD (2016) Hybrid organic–inorganic H<sub>2</sub>-evolving photocathodes: understanding the route towards high performance organic photoelectrochemical water splitting. *J Mater Chem A* 4:2178–2187
  11. Vu QT, Pavlik M, Hebestreit N, Rammelt U, Plieth W, Pflieger J (2005) Nanocomposites based on titanium dioxide and polythiophene: structure and properties. *ReacFuncPolym* 65:69–77
  12. Habelhames F, Lamiri L, Zerguine W, Nessark B (2013) Improvement of photoelectrochemical and optical characteristics of MEH-PPV using titanium dioxide nanoparticles. *Mater Sci Semicond Process* 16:727–731. <https://doi.org/10.1016/j.mssp.2012.12.015>
  13. Habelhames F, Zerguine W, Lamiri L, Nessark B, Derbal-Habak H (2013) Morphology and photoelectrochemical characterization of MEH-PPV/PCBM composite film doped with TiO<sub>2</sub> nanoparticles. *Acta Metall Sin (Engl Lett)* 26:373–377. <https://doi.org/10.1007/S40195-012-0269-z>
  14. Rojas HC, Bellani S, Sarduy EA, Fumagalli F, Mayer MT, Schreier M, Grätzel M, Fozzo FD, Antognazza MR (2017) All solution-processed, hybrid organic–inorganic photocathode for hydrogen evolution. *ACS Omega* 2:3424–3431. <https://doi.org/10.1021/acsomega.7b00558>
  15. Derbal-Habak H, Bergeret C, Cousseau J, Nunzi JM (2011) Improving the current density J<sub>sc</sub> of organic solar cells P3HT:PCBM by structuring the photoactive layer with functionalized SWCNTs. *Sol Energy Mater Sol Cells* 95:S53–S56
  16. Pathak D, Wagner T, Adhikari T, Nunzi JM (2015) Photovoltaic performance of AgInSe<sub>2</sub> conjugated polymer hybrid system bulk heterojunction solar cells. *Synthetic Metals* 199:87–92
  17. Jabeen U, Adhikari T, Mujtaba Shah S, Pathak D, Wagner T, Nunzi JM (2017) Influence of the dopant concentration on structural, optical and photovoltaic properties of Cu-doped ZnS nanocrystals based bulk heterojunction hybrid solar cells. *Eur Phys J Appl Phys* 78:34811
  18. Irwin MD, Buchholz DB, Hains AW, Chang RPH, Marks TJ (2008) P-type semiconducting nickel oxide as an efficiency-enhancing anode interfacial layer in polymer bulk-heterojunction solar cells. *PNAS* 105:2783–2787. <https://doi.org/10.1073/pnas.0711990105>
  19. Chapel A, Dkhil SB, Therias S, Gardette JL, Hannani D, Poize G, Gaceur M, Shah SM, Chung PWW, Ackermann CV, Margeat O, Rivaton A, Ackermann J (2016) Effect of ZnO nanoparticles on the photochemical and electronic stability of P3HT used in polymer solar cells. *Sol Energy Mater Sol Cells* 155:79–87. <https://doi.org/10.1016/j.solmat.2016.04.052>
  20. Gonçalves R, Moraes FC, Pereira EC (2016) Reduced graphene oxide enhancing the photoelectrochemical properties of poly(3-hexylthiophene). *Carbon* 109:57–64. <https://doi.org/10.1016/j.carbon.2016.07.041>
  21. Wang G, Hirasa T, Moses D, Heeger AJ (2004) Fabrication of regioregular poly(3-hexylthiophene) field-effect transistors by dip-coating. *Synth Met* 146:127–132. <https://doi.org/10.1016/j.synthmet.2004.06.026>
  22. Villers BT, Tassone CJ, Tolbert SH, Schwartz BJ (2009) Improving the reproducibility of P3HT:PCBM solar cells by controlling the PCBM/cathode interface. *J Phys Chem C* 113:18978–18982. <https://doi.org/10.1021/jp9082163>
  23. Loheeswaran S, Thanihachelvan M, Ravirajan P, Nelson J (2017) Controlling recombination kinetics of hybrid poly-3-hexylthiophene (P3HT)/titanium dioxide solar cells by self-assembled monolayers. *J Mater Sci Mater Electron* 28:4732–4737
  24. Liu H, Li M, Yang J, Hu C, Shang J, Zhai H (2018) In situ construction of conjugated polymer P3HT coupled hierarchical ZnO composite with Z-scheme enhanced visible-light photocatalytic activity. *Mater Res Bull* 106:19–27. <https://doi.org/10.1016/j.materresbull.2018.05.026>
  25. Zhang W, Nguyen NA, Murray R, Xin J, Mackay ME (2017) A comparative study on the morphology of P3HT:PCBM solar cells with the addition of Fe<sub>3</sub>O<sub>4</sub> nanoparticles by spin and rod coating methods. *J Nanopart Res* 19:315–323
  26. Yu XX, Yin H, Li HX, Zhang W, Zhao H, Li C, Zhu MQ (2017) Piezo-phototronic effect modulated self-powered UV/visible/near-infrared photodetectors based on CdS: P3HT microwires. *Nano Energy* 34:155–163. <https://doi.org/10.1016/j.nanoen.2017.02.033>
  27. Heo K, Miesch C, Na JH, Emrick T, Hayward RC (2018) Assembly of P3HT/CdSe nanowire networks in an insulating polymer host. *Soft Matter* 14:5327–5332. <https://doi.org/10.1039/C8SM01001C>
  28. Heo K, Miesch C, Na JH, Emrick T, Hayward RC (2018) Assembly of P3HT/CdSe nanowire networks in an insulating polymer host. *Soft Matter* 3:1525–1533. <https://doi.org/10.1039/C8SM01001C>
  29. Ikram M, Imran M, Nunzi JM, Bobbara SR, Ali S, U-Din I (2015) Efficient and low cost inverted hybrid bulk heterojunction solar cells. *J Renewable Sustain Energy* 7:043148
  30. Chan IM, Hong FC (2004) Improved performance of the single-layer and double-layer organic light emitting diodes by nickel oxide coated indium tin oxide anode. *Thin Solid Films* 450:304–311. <https://doi.org/10.1016/j.tsf.2003.10.022>
  31. Chtouki T, Soumahoro L, Kulyk B, Erguig H, Elidrissi B, Sahraoui B (2017) Spin-coated tin-doped NiO thin films for third order non linear optical applications. *Optik* 136:237–243. <https://doi.org/10.1016/j.ijleo.2017.01.110>
  32. Nguyen DT, Ferrec A, Keraudy J, Bernède JC, Stephant N, Cattin L, Jouan PY (2014) Effect of the deposition conditions of NiO anode buffer layers in organic solar cells, on the properties of these cells. *Appl Surf Sci* 311:110–116. <https://doi.org/10.1016/j.apsusc.2014.05.020>
  33. Wu MS, Huang YA, Yang CH, Jow JJ (2007) Electrodeposition of nanoporous nickel oxide film for electrochemical capacitors. *Int J Hydrog Energy* 32:4153–4159. <https://doi.org/10.1016/j.ijhydene.2007.06.001>
  34. Jamal RK, Naji I (2016) Electrical properties of pure NiO and NiO: Au thin films prepared by using pulsed laser deposition. *Iraqi J Phys* 14:37–43 [www.iasj.net/iasj?func=article&aid=115237](http://www.iasj.net/iasj?func=article&aid=115237)
  35. Bandara J, Divarathne CM, Nanayakkara SD (2004) Fabrication of n–p junction electrodes made of n-type SnO<sub>2</sub> and p-type NiO for control of charge recombination in dye sensitized solar cells. *J Solar Energy Mater Solar Cells* 81:429–437. <https://doi.org/10.1016/j.solmat.2003.11.027>

36. Srinivasan V, Weidner JW (1997) An electrochemical route for making porousnickel oxide electrochemical capacitors. *Electrochem Soc* 144:210–213. <https://doi.org/10.1149/1.1837859>
37. Gupta A, Akhtar AJ, Saha SK (2013) In-situ growth of P3HT/graphene composites for supercapacitor application. *J Mater Chem Phys* 140(1–6):616–621. <https://doi.org/10.1016/j.matchemphys.2013.04.015>
38. Lou X, Zhao X, He X (2009) Boron doping effects in electrochromic properties of NiO films prepared by sol–gel. *J Solar Energy* 83:2103–2108. <https://doi.org/10.1016/j.solener.2009.06.020>
39. Xia XH, Tu JP, Zhang J, Wang XL, Zhang WK, Huang H (2008) Electrochromic properties of porous NiO thin films prepared by a chemical bath deposition. *J Solar Energy Mater Solar Cells* 92:628–633. <https://doi.org/10.1016/j.solmat.2008.01.009>
40. Patil PS, Kadam LD (2002) Preparation and characterization of spray pyrolyzed nickel oxide (NiO) thin films. *Appl Surf Sci* 199: 211–221. [https://doi.org/10.1016/S0169-4332\(02\)00839-5](https://doi.org/10.1016/S0169-4332(02)00839-5)
41. Chrissanthopoulos A, Baskoutas S, Bouropoulos N, Dracopoulos V, Pouloupoulos P, Yannopoulos SN (2011) Synthesis and characterization of ZnO/NiO p–n heterojunctions: ZnO nanorods grown on NiO thin film by thermal evaporation. *J Photonics Nanostruct Fundam Appl* 9:132–139. <https://doi.org/10.1016/j.photonics.2010.11.002>
42. Lu YM, Hwang WS, Yang JS, Chuang HC (2002) Properties of nickel oxide thin films deposited by RF reactive magnetron sputtering. *Thin Solid Films* 420–421:54–61. [https://doi.org/10.1016/S0040-6090\(02\)00654-5](https://doi.org/10.1016/S0040-6090(02)00654-5)
43. Sonavane AC, Inamdar AI, Shinde PS, Deshmukh HP, Patil RS, Patil PS (2010) Efficient electrochromic nickel oxide thin films by electrodeposition. *J Alloys Compd* 489:667–673. <https://doi.org/10.1016/j.jallcom.2009.09.146>
44. Wu K, Zhao J, Wu R, Ruan B, Liu H, Wu M (2018) The impact of Fe<sup>3+</sup> doping on the flexible polythiophene electrodes for supercapacitors. *J Electroanal Chem* 823:527–530. [doi.org/10.1016/j.jelechem.2018.06.052](https://doi.org/10.1016/j.jelechem.2018.06.052)
45. Manoli K, Dumitru LM, Mulla MY, Magliulo M, Franco CD, Santacroce MV, Scamarcio G, Torsi L (2014) A comparative (2014) study of the gas sensing behavior in P3HT-and PBTTT-based OTFTs: the influence of film morphology and contact electrode position. *Sensors* 14:16869–16880. <https://doi.org/10.3390/s140916869>
46. Giannopoulos P, Andreopoulou AK, Lianos P, Nikolakopoulou A, Sygellou L, Kallitsis JK (2014) An alternative methodology for anchoring organic sensitizers onto TiO<sub>2</sub> semiconductors for photoelectrochemical applications. *J Mater Chem* 2:20748–20759. <https://doi.org/10.1039/c4ta04515g>
47. Wu F, Shan Y, Wang R, Zhu L (2016) Incorporation of diketopyrrolopyrrole dye to improve photovoltaic performance of P3HT: PCBM based bulk heterojunction polymer solar cells. *Org Electron* 31:171–176. <https://doi.org/10.1016/j.orgel.2016.01.028>
48. Kruef V, Wisitsoraat A, Tuantranont A, Phanichphant S (2014) Gas sensing properties of conducting polymer/Au-loaded ZnO nanoparticle composite materials at room temperature. *Nanoscale Res Lett* 9:467–479
49. Tullii G, Desii A, Bossio C, Bellani S, Colombo M, Martino N, Antognazza MR, Lanzani G (2017) Bimodal functioning of a mesoporous, light sensitive polymer/electrolyte interface. *Org Electron* 46:88–98. <https://doi.org/10.1016/j.orgel.2017.04.007>
50. Adhikari T, Bobbara SR, Nunzi JM, Lebel O (2018) Efficiency enhancement of ternary blend organic photovoltaic cells with molecular glasses as guest acceptors. *Org Electr* 53:74–82
51. Bielecka U, Lutsyk P, Janus K, Sworakowski J, Bartkowiak W (2011) Effect of solution aging on morphology and electrical characteristics of regioregular P3HT FETs fabricated by spin coating and spray coating. *Org Electron* 12:1768–1776. <https://doi.org/10.1016/j.orgel.2011.06.027>
52. Chang H, Wang P, Li H, Zhang J, Yan D (2013) Solvent vapor assisted spin-coating: a simple method to directly achieve high mobility from P3HT based thin film transistors. *Synth Met* 184:1–4. <https://doi.org/10.1016/j.synthmet.2013.09.031>
53. Gollu SR, Sharma R, Srinivas G, Kundu S, Gupta D (2014) Effects of incorporation of copper sulfide nanocrystals on the performance of P3HT: PCBM based inverted solar cells. *Org Electron* 15:2518–2525. <https://doi.org/10.1016/j.orgel.2014.06.035>
54. Al-Ghamdi AA, Mahmoud WE, Yaghmour SJ, Al-Marzouki FM (2009) Structure and optical properties of nanocrystalline NiO thin film synthesized by sol–gel spin-coating method. *J Alloys Compd* 486:9–13. <https://doi.org/10.1016/j.jallcom.2009.06.139>
55. Wang J, Wei L, Zhang L, Jiang C, Kong ESW, Zhang Y (2012) Preparation of high aspect ratio nickel oxide nanowires and their gas sensing devices with fast response and high sensitivity. *J Alloys Compd* 22:8327–8335. <https://doi.org/10.1039/C2JM16934G>
56. El-Kemary M, Nagy N, El-Mehasseb I (2013) Nickel oxide nanoparticles: synthesis and spectral studies of interactions with glucose. *Mater Sci Semicond Process* 16:1747–1752. <https://doi.org/10.1016/j.mssp.2013.05.018>
57. Kim TH, Jeon HJ, Lee JW, Nah YC (2015) Enhanced electrochromic properties of hybrid P3HT/WO<sub>3</sub> composites with multiple colorations. *Electrochem Commun* 57:65–69. <https://doi.org/10.1016/j.elecom.2015.05.008>
58. HabElhames F, Nessark B, Boumaza N, Bahloul A, Bouhafis D, Cheriet A (2009) Electrochemical and photoelectrochemical study of gallium arsenide–polybithiophene composite. *Synth Met* 159: 1349–1352. <https://doi.org/10.1016/j.synthmet.2009.03.009>